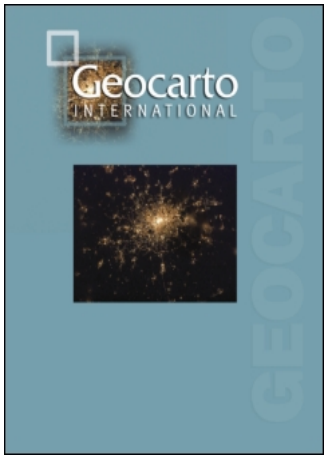

Geocarto International
Publication details, including instructions for authors and subscription information:
http://www.informaworld.com/smpp/title~content=t759156373

Spectroscopic determination of health levels of coast live oak (**Quercus agrifolia**) leaves

R. Pu [a]; M. Kelly [b]; Q. Chen [b]; P. Gong [b]
[a] Department of Geography, University of South Florida, Tampa, FL, USA
[b] Center for Assessment & Monitoring of Forest & Environmental Resources (CAMFER), 145 Mulford Hall, University of California, Berkeley, CA, USA

First Published on: 24 October 2007
To cite this Article: Pu, R., Kelly, M., Chen, Q. and Gong, P. (2007) 'Spectroscopic determination of health levels of coast live oak (**Quercus agrifolia**) leaves', Geocarto International, 23:1, 3 - 20
To link to this article: DOI: 10.1080/10106040701417220
URL: http://dx.doi.org/10.1080/10106040701417220

Geocarto International
Vol. 23, No. 1, February 2008, 3–20

Spectroscopic determination of health levels of coast live oak (*Quercus agrifolia*) leaves

R. PU*†, M. KELLY‡, Q. CHEN‡ and P. GONG‡
†Department of Geography, University of South Florida, 4202 E. Fowler Ave., NES 107, Tampa, FL 33620, USA
‡Center for Assessment & Monitoring of Forest & Environmental Resources (CAMFER), 145 Mulford Hall, University of California, Berkeley, CA 94720-3114, USA

(*Received 24 November 2005; in final form 20 February 2007*)

Three sets of coast live oak (*Quercus agrifolia*) leaf samples were collected on three dates: 20 April 2002, 23 July 2002 and 11 September 2001, respectively, for Sudden Oak Death (SOD) monitoring. A total of 330 reflectance spectra (covering 350–2500 nm) were measured in the laboratory with a spectrometer FieldSpec®Pro FR. In this study, the spectroscopic determination of two health levels of the coast live oak leaves was conducted with three sets of spectra. We used two classification algorithms, penalized discriminant analysis (PDA) and cross correlogram spectral matching (CCSM), to discriminate between healthy and infected leaves. PDA is a penalized version of Fisher's linear discriminant analysis (LDA) and can considerably improve upon LDA when it is used for the classification of hyperspectral data. CCSM is practised by calculating the cross correlation at different match positions between a test spectrum and a reference spectrum and is also suitable for processing hyperspectral data. Experimental results indicate that the PDA algorithm has produced approximately 7% higher classification accuracy than that produced by CCSM, although both are very low. When considering the subtle spectral differentiation between the two health levels, the PDA method demonstrates its promise as a classification algorithm. Among the 10 spectral ranges, some higher accuracies are produced by both PDA and CCSM algorithms from those spectral range wavelengths shorter than 1400 nm. Based on our experimental results and previous work, existing remote sensing techniques, including airborne or satellite remote sensing and multispectral or hyperspectral remote sensing, may be insufficient for monitoring and mapping disease-induced moisture stress in trees that have recently been infected. However, this does not preclude the analysis of trees at very advanced stages of disease, and the practicality of finding trees within weeks of dying is considerable.

Keywords: Spectroscopic analysis; Sudden Oak Death (SOD); Coast live oak; Penalized discriminant analysis (PDA); Cross correlogram spectral matching (CCSM)

*Corresponding author. Email: rpu@cas.usf.edu

Geocarto International
ISSN 1010-6049 print/ISSN 1752-0762 online © 2008 Taylor & Francis
http://www.tandf.co.uk/journals
DOI: 10.1080/10106040701417220

1. Introduction

A new disease affecting several tree and shrub species in coastal California USA, commonly called Sudden Oak Death (SOD), is caused by a newly discovered virulent pathogen called *Phytophthora ramorum* (Rizzo *et al*. 2002). The disease has two forms: a trunk canker form that affects several tree species and in many cases causes death, and a non-lethal foliar form that affects several other trees as well as shrubs. Over the past eight years, a large number of coast live oak (*Quercus agrifolia*), tanoak (*Lithocarpus densiflorus*) and black oak (*Q. kelloggii*) trees have been killed by this disease (McPherson *et al*. 2000, Garbelotto *et al*. 2001). In addition to a suite of symptoms found on the trunks of those infected trees, once crown dieback begins, the foliage of infected trees appears to die rapidly, changing colour from dark green to pale yellow to brown within a few weeks (McPherson *et al*. 2000, Garbelotto *et al*. 2001). In order to monitor the occurrence and spread of the SOD disease in California, high-resolution imagery (Airborne Acquisition and Registration Imagery, ADAR) has been used to map dead and dying oak trees in a study area in Marin County, California (Kelly 2002, Kelly and Meentemeyer 2002).

Similarly, Everitt *et al*. (1999) reported that they could detect oak wilt disease in south-central Texas, USA, using airborne digital imagery. They found that they could delineate dead, diseased, and healthy live oak trees on the digital imagery. These efforts prove that multispectral remotely sensed imagery captured by airborne sensors can detect oak mortality caused by disease. This is due to the fact that the spectral characteristics of diseased oak leaves significantly differ from those of healthy trees. These spectral differences can be caused by changes in major pigment concentrations and water content contained in oak leaves (Everitt *et al*. 1999, Pu *et al*. 2003, 2004).

In addition to mapping mortality, it is a prudent goal to attempt to diagnose SOD infected oak trees at a much earlier stage, before the leaves have undergone dramatic shifts in pigmentation. Success in mapping infected or stressed trees would lend managers significant advantages in dealing with the disease. Treatment might be utilized, or at least hazard trees could be monitored. In our initial examination of this problem, we suspected that the foliage of infected trees had a different water status from healthy leaves even when they appear green. If this is true, the infected foliage might have different spectral characteristics from healthy leaves although this difference might possibly be subtle. This led us to examine the spectral difference using spectral reflectance measured in the laboratory from oak leaves gathered from healthy and infected coast live oak trees.

We have known that the spectral difference between the two health levels of oak leaves sampled is very slight (Pu *et al*. 2003, 2004) (figure 1) due to the similar relative water contents (RWCs) of green oak leaves between the two health levels. From the scarce literature on possible spectral differences between the two health levels due to other biochemical constituent changes in the infected leaves (Rizzo *et al*. 2002, Skiecki and Bernhardt 2002), we assumed the slight spectral difference between the two health levels might be mainly caused by the difference in the RWCs of oak leaves at the two health levels, even though the RWC difference is very small.

To detect SOD spectrally, especially at the early infected stage, we proposed the application of some advanced classification algorithms that are suitable for processing hyperspectral data in studying the potential of the subtle spectral difference between the two health levels of oak leaves for identifying the SOD-infected oak trees with the laboratory-measured spectral data. Of the existing

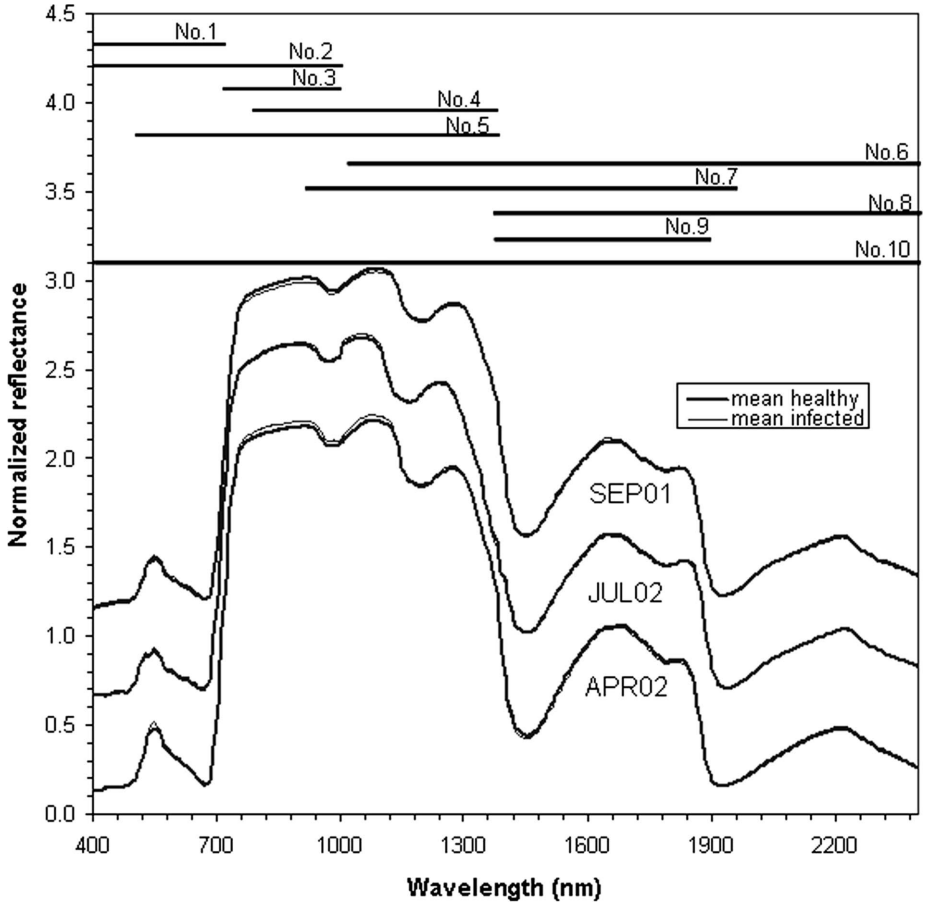

Figure 1. Mean reflectance spectra of the two health levels from the three spectral datasets (APR02, JUL02 and SEP01) showing slight differences in average spectra between the two health levels: healthy and infected. Note that the mean spectra between the three datasets have been displaced vertically by 0.5 units to avoid overlapping. Spectral region numbers and spectral ranges are given in tables 2 and 4.

classification algorithms, we selected two newly developed algorithms to test their discriminant power for spectroscopic determination of the two health levels of coast live oak leaves with laboratory-measured spectra in this study. The two algorithms are penalized discriminant analysis (PDA) and cross correlogram spectral matching (CCSM). PDA is a penalized version of Fisher's linear discriminant analysis (LDA) and can considerably improve upon LDA when it is used for the classification of hyperspectral data (Hastie *et al.* 1995, Yu *et al.* 1999). Yu *et al.* (1999) used the technique to identify six conifer species with *in-situ* hyperspectral measurements and obtained almost double the accuracy of the LDA. CCSM is practised by calculating the cross correlation at different match positions between a test spectrum and a reference spectrum. A test spectrum with a higher cross correlation will have a perfect matching to a reference spectrum, which leads to the test spectrum being classified to the reference spectrum. Van der Meer and Bakker (1997, 1998) have employed the algorithm in mapping surface mineralogical materials with Airborne

Visible/Infrared Imaging Spectrometer (AVIRIS) data in Cuprite, Nevada and they successfully mapped three minerals there—kaolinite, alunite and buddingtonite. Although the CCSM algorithm was initially tested for differentiating mineralogical materials (Van der Meer and Bakker 1997, 1998), a task somewhat different from our identification of the health levels of oak leaves, based on the principle of the CCSM algorithm, we can apply the algorithm in this analysis. Furthermore, given hyperspectral measurements of oak leaves, we expect that the CCSM will be able to efficiently use the similarity of spectral shape among individual spectra at one health level to separate the two spectral groups, corresponding to the two heath levels.

To spectrally distinguish infected trees from healthy trees using laboratory-measured hyperspectral data, it is better to explore all spectral ranges. In this study, we focused on 10 spectral ranges, some of which overlapped, in considering complete spectral properties in an individual range along the spectral range of 400–2500 nm. We first performed several preprocessing routines to the three spectral datasets taken at three different seasons. These included band smoothing, neighbour band merging and illumination normalization. Subsequently, the two spectrally discriminant algorithms (PDA and CCSM) were used to test spectral identification of the two health levels. Our experimental objectives included: (1) to test and compare the discriminant power of the two algorithms in identifying the two health levels: healthy and infected, and (2) to discuss the potential for using laboratory spectra or advanced remote sensing data to diagnose SOD symptoms appearing on oak canopy at early stages.

2. Field sampling and data measurement

2.1 *Leaf sampling*

A total of 330 coast live oak leaf samples were collected in three seasons—late spring (rainy season, 20 April 2002), summer (dry season, 23 July 2002) and early fall (very dry season, 11 September 2001)—at China Camp State Park (122°29′50″ W, 38°00′30″ N), Marin County, CA, USA. All leaf samples were divided into three datasets, called APR02 (spring), JUL02 (summer) SEP01 (early fall) (table 1). In order to reduce the effects of any high variability of water content in both healthy and infected leaves on sample spectra, leaf samples were randomly collected from branches at different canopy surface positions from different trees. For each tree canopy three samples were collected and all leaf samples consisted of fresh green leaves. Green leaf samples included the two health levels: healthy (trees with no apparent SOD symptoms on the trunk) and infected (trees showing the characteristic 'bleeding' on the trunk, an indication of SOD (Rizzo *et al.* 2002)).

The leaf samples were collected in the field and were immediately sealed in plastic bags, then sent to the laboratory at the University of California at Berkeley for spectral reflectance measurement with a FieldSpec®ProFR (Analytical Spectral Devices, Inc., Boulder, CO, USA) within half a day. With this method, we did not

Table 1. A breakdown of the three spectral datasets.

Dataset	Healthy	Infected	Total	Measuring date
APR02	46	50	96	20 April 2002
JUL02	60	66	126	23 July 2002
SEP01	54	54	108	11 September 2001

find any significant spectral difference between similar samples collected at both the beginning and the end and spectrally measured within the half day. After the spectral measurement of each leaf sample, the leaves were immediately weighed with an electronic scale. They were then dried for the second weighing.

2.2 *Reflectance measurement*

Spectral measurements of all oak leaf samples were measured with the same spectrometer by following the same procedure. The FieldSpec®ProFR covers the spectral range of 350–2500 nm, consisting of three separate spectrometers. The first spectrometer has a spectral resolution of 3 nm and the second and third have the same spectral resolution of approximately 10 nm. All spectra were measured at the nadir direction of the radiometer with a 25° field of view (FOV). Lighting is achieved with two 500 W halogen tungsten filament lamps. The distance between the spectrometer and the leaf samples was about 5 cm to ensure within-leaf area radiance measurement. White reference was measured every 5–10 minutes. Each leaf sample consisted of an overlapped piling of 5–10 leaves to eliminate the possible effect of background (black cloth) on the spectrum (based on our experiment, a reflectance spectrum of an overlapped piling of five oak leaves becomes stable). Each sample was repeatedly measured 10 times with the spectrometer, five from the adaxial surface and five from the abaxial surface, in order to obtain an average spectral curve for each sample.

2.3 *Relative water content (RWC)*

Every oak leaf sample was immediately weighed after spectral measurement (Fresh Weight, FW). Then they were dried in an oven at 65°C until constant weight (Dry Weight, DW) was reached. Finally, the relative water content (RWC, %) was calculated from $\mathrm{RWC} = 100(\mathrm{FW} - \mathrm{DW})/\mathrm{FW}$.

3. Analysis method

3.1 *Data preprocessing*

For testing spectroscope determination of the two health levels with all spectral samples, we performed the following preprocessing on the three spectral datasets. First, each spectral curve was truncated with a band wavelength shorter than 400 nm and longer than 2400 nm because these two-end spectral data were too noisy to be used, leaving 2001 bands for subsequent analysis. Second, we smoothed each spectral curve using a 5-band smoothing, which is similar to a low pass filtering. We then merged every five neighbouring bands into one by an arithmetic average calculation, yielding 401 bands for each spectrum with a bandwidth of 5 nm. Next, the spectral curve was normalized by band reflectance divided by the mean reflectance of the spectrum. That is, we replaced a band reflectance ρ_i with $\rho_i \Big/ \left(\frac{1}{401}\sum_{i=1}^{401}\rho_i\right)$. The effectiveness of such normalization is the suppression of illumination changes among different measurements (Gong *et al*. 2001). In this spectral preprocessing, the spectral smoothing and averaging applied to the datasets did not cause a removal of some of the subtle spectral differences due to different health levels of oak leaves, based on

the following two points. Firstly, we checked the ratio of signal-to-noise (SNR) with different smoothing (filter) sizes of 3, 5, 7 and 9 bands. We found that the use of 5-band smoothing obtained the greatest SNR. It is true that when a smoothing is executed on a spectrum, some degree of subtle spectral signal may be removed, but removal of the spectral noise may be a major part. It is important to make a better trade-off for removing as much noise as possible. Secondly, the spectrometer we used is the FieldSpec®ProFR, which covers the spectral range of 350 nm to 2500 nm, consisting of three separate spectrometers. The first spectrometer has a spectral resolution of 3 nm and the second and third have the same spectral resolution of approximately 10 nm. Although the output spectral bandwidth from the instrument is 1 nm, they are interpolated from 3 nm and 10 nm original spectral resolutions. So, averaging to 5 bandwidth data may not compress the subtle spectral information. Actually, we tested the APR02 dataset in its original 1 nm bandwidth and did not find any improvement in identification accuracy of the two health levels.

3.2 *Algorithms*

3.2.1 PDA. Fisher's linear discriminant analysis (LDA) is a standard tool used both for classification and dimension reduction. However, according to Hastie *et al.* (1995), LDA also has two deficiencies. First, LDA is too flexible in situations with a large number of highly correlated predictor variables (such as our spectral samples with 401 bands), and second, it is too rigid in situations where the class boundaries in predictor space are complex and nonlinear. In the first case, LDA overfits and in the second case, it underfits the data. To improve the performance of LDA and overcome both the problems abovementioned, Hastie *et al.* (1995) added a penalty term to the within class variance matrix Σ_w as:

$$\Sigma'_w = \Sigma_w + \Omega, \tag{1}$$

where Σ'_w is a within class covariance matrix after adding a penalty matrix Ω. The selection and discussion of Ω is found in Hastie *et al.* (1995).

In order to recognize six confer species using *in-situ* hyperspectral measurements with the PDA analysis technique, Yu *et al.* (1999) considered two types of penalty matrix. One is a second derivative-type penalty matrix Ω_D for penalizing high local variation. This type of penalty matrix may be defined as:

$$\Omega_D = \lambda D_K^T D_{K-1}^T D_{K-1} D_K \tag{2}$$

where D_K denotes $K-1$ by K-dimensional first difference operator matrix; and λ is called the smoothing parameter. The second is a shrinkage-type penalty that takes the form,

$$\Omega_S = \lambda I_K \tag{3}$$

where I_K is the $K \times K$ identity matrix. This is analogous to ridge regression analysis. For the geometric interpretation of Ω_S and the design of Ω_D, refer to Yu *et al.* (1999). In this study, we tested the second derivative penalty matrix Ω_D, because it can penalize high local variation associated with some bands,

particularly those bands located at and around the areas joining the three spectrometers. Also, its penalty effectiveness had been demonstrated in Yu *et al.* (1999). For preventing the penalty Ω_D from creating unstable results, we also need to ridge the penalty to increase stability. Since similar spectral characteristics exist between the dataset (describing similar spectral characteristics of six conifer species) analysed by Yu *et al.* (1999) and the dataset (spectral characteristics also being very similar between the two health levels of oak leaves) used in this analysis, we expected that we could obtain results similar to those produced by Yu *et al.* (1999) when using the PDA algorithm with Ω_D in this analysis. The PDA discriminant analysis was performed in Splus using the MDA() collection of functions written by Hastie and Tibshirani. These functions are documented and publicly available from the S archive of StatLib at http://lib.stat.cmu.edu.

3.2.2 CCSM. The cross correlogram spectral matching (Van der Meer and Bakker 1997, 1998) is practised by calculating a set of cross correlation coefficients at different match positions between a test spectrum (an unknown spectrum or a pixel spectrum) and a reference spectrum (a known or laboratory measurement spectrum). According to the method provided by Van der Meer and Bakker (1997, 1998), we moved the test spectrum and referred to a negative match position when shifting towards a shorter wavelength and to a positive match position when shifting towards a longer wavelength. Thus match position +1 means that we are calculating the cross correlation coefficient between the reference spectrum and the test spectrum in which all bands have been shifted by one band position number towards the shorter wavelength end of the test spectrum. The cross correlation is equivalent to a linear correlation coefficient calculated with a set of overlapping bands after shifting. Therefore, a cross correlation for matching position m can be calculated as:

$$r_m = \frac{n\Sigma R_r R_t - \Sigma R_r \Sigma R_t}{\sqrt{[n\Sigma R_r^2 - (\Sigma R_r)^2][n\Sigma R_t^2 - (\Sigma R_t)^2]}} \tag{4}$$

where R_r, R_t are reference and test spectrum, respectively; n is the number of overlapping bands. The significance of the r_m can be assessed with the following t-test:

$$t = r_m \sqrt{\frac{n-2}{1-r_m^2}} \tag{5}$$

If $t > t_\alpha\,(n-2)$ then r_m is significant at $(1-\alpha)$ confidence level.

A test spectrum with a higher cross correlation will be perfectly matched to a reference spectrum, which leads to the test spectrum classified to the reference spectrum. Figure 2 illustrates an application example of the CCSM with our spectral data of coast live oak leaves. The figure demonstrates that the test spectrum should be classified as the infected level because it has higher cross correlogram value with infected reference spectrum than that with healthy spectrum. Furthermore, the cross correlogram is symmetric about the match position zero. Generally, the cross

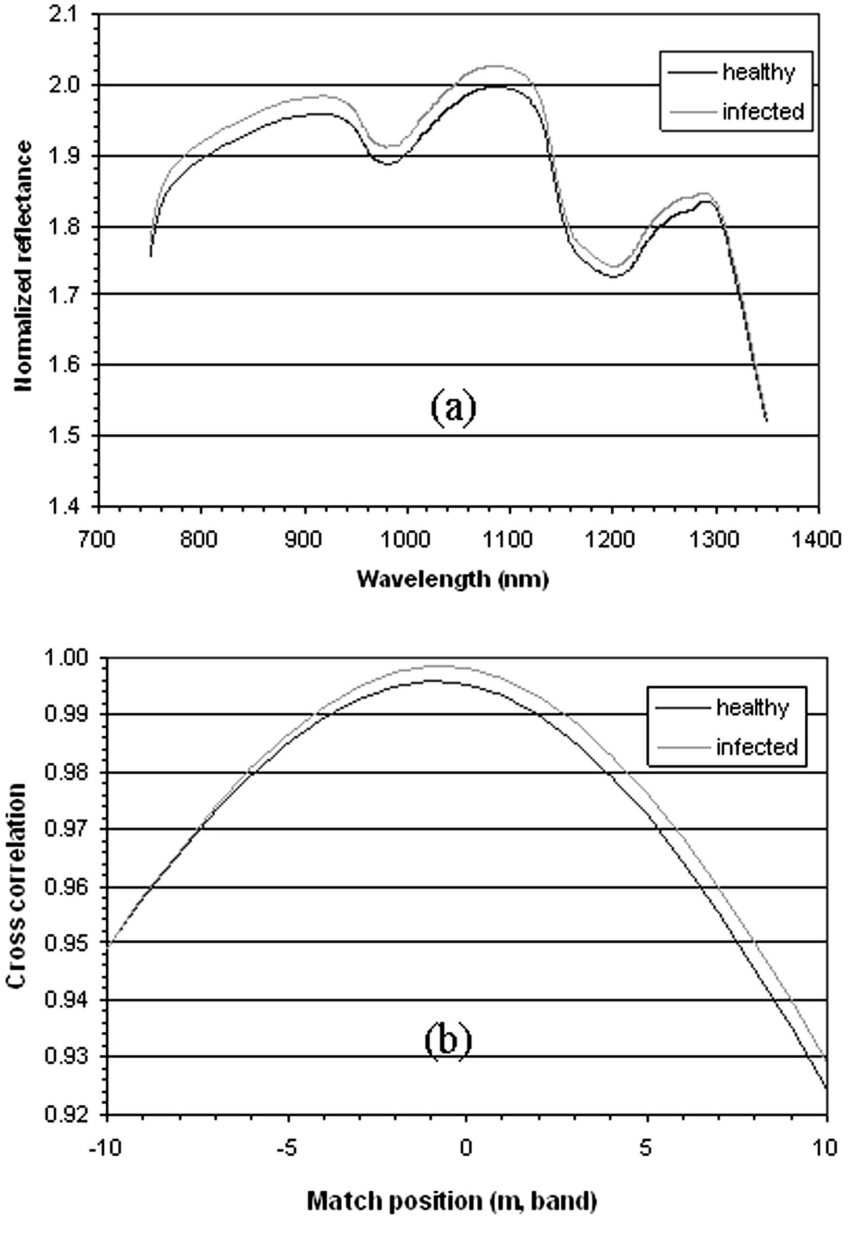

Figure 2. Part mean spectra (*a*) of training spectral sets as references for the two health levels and corresponding cross correlograms (*b*) calculated from a test spectrum that is measured from an infected leaf sample with the reference spectra in (*a*). The grey line in (*b*) indicates that the test spectrum has matched with the infected reference spectrum better than with the healthy reference spectrum. So the test spectrum should be classified to the infected level.

correlogram for perfectly matching reference and test spectra is a parabola around the central matching number ($m = 0$) with a peak correlation of 1 (Van der Meer and Bakker 1997). The CCSM algorithm was written in Matlab script and run in Matlab in this test.

3.3 *Spectral ranges*

In this study, in addition to testing the seasonal effect on identification of the two health levels with laboratory-measured spectra, we also tested the effect of different spectral ranges on identification accuracy. The spectral ranges were separated based on plant spectral characteristics, i.e. several major absorption and reflected characteristics. A total of 10 spectral ranges (see wavelength ranges in table 2 and figure 1) were tested. They cover approximately three varying spectral ranges with distinguished spectral features: the visible region with major pigment absorption (e.g. chlorophyll content), the near infrared (NIR) region with highly reflected features (caused by cell structure and multi-reflected properties), and the short wave infrared (SWIR) region with multi-biochemicals (e.g. water content). The SWIR region was further divided into two ranges with one containing two minor water absorption features (SWIR1, covering $\sim$1000–1300 nm) and the other covering two major water absorption features (SWIR2, covering $\sim$1300–2400 nm). Some spectral ranges have combined two neighbouring features, such as, visible + NIR, NIR + SWIR1, NIR + SWIR. Finally, the last one covers the full range (400–2400 nm).

4. Results and analysis

4.1 *PDA*

Each of the three sets of spectral measurements (table 1) was used to test PDA performance. We calculated classification accuracies using PDA with the second derivative penalty matrix Ω_D for each spectral dataset from 10 spectral ranges. For each dataset, we first tested a range of values for the smoothing parameter λ to determine an optimal λ value, then applied the λ value to calculate classification accuracies for all 10 spectral ranges. The optimal λ values are 1.0, 0.5 and 0.1,

Table 2. Discriminant accuracies of three datasets at the two health levels using PDA classifier.

		APR02, $\lambda = 1.0$, N = 96			JUL02, $\lambda = 0.5$, N = 126			SEP01, $\lambda = 0.1$, N = 108		
No.	Wavelength range (nm)	H-rate	I-rate	H-I ave	H-rate	I-rate	H-I ave	H-rate	I-rate	H-I ave
1	400–702	0.52	*0.75*	0.646	0.62	0.68	0.651	*0.67*	0.54	0.602
2	400–1002	*0.67*	0.72	*0.698*	*0.73*	*0.80*	*0.770*	0.59	0.59	0.593
3	707–1002	0.61	0.60	0.604	0.58	0.64	0.611	0.57	*0.80*	0.602
4	782–1372	0.61	0.68	0.646	0.58	0.67	0.627	0.59	*0.67*	0.630
5	502–1372	*0.67*	0.70	0.687	*0.67*	*0.76*	*0.714*	0.60	0.63	0.611
6	1007–2400	0.61	0.68	0.646	0.50	0.64	0.571	*0.69*	0.63	*0.658*
7	852–1897	0.65	0.72	0.687	0.63	0.68	0.659	0.63	0.61	0.620
8	1377–2400	0.61	0.70	0.656	0.38	0.65	0.524	0.57	0.54	0.556
9	1377–1897	0.63	0.66	0.646	0.43	0.62	0.532	0.52	0.65	0.583
10	400–2400	*0.76*	*0.74*	*0.750*	0.63	0.71	0.675	0.63	*0.67*	*0.648*
	Average	0.634	0.695	0.667	0.575	0.685	0.633	0.606	0.633	0.610

Note: H-rate and I-rate denote discriminant accuracies from healthy and infected samples, respectively; H-I ave is average of H-rate and I-rate. The italic numbers in the table indicate the first and second highest accuracy in each column.

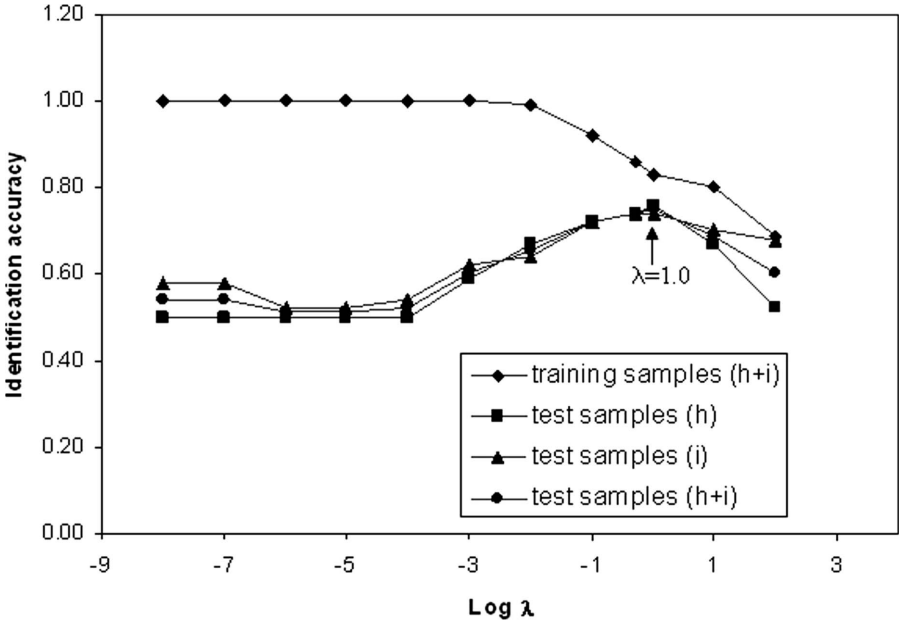

Figure 3. Discriminant accuracy as a function of smoothing parameter λ, generated from the APR02 spectral dataset. The four curves from top to bottom are identification accuracies calculated from healthy and infected training samples, from healthy test samples alone, from infected test samples alone and from healthy and infected test samples.

respectively for datasets APR02, JUL02 and SEP01. Figure 3 shows the classification accuracy produced from the APR02 dataset for PDA with the second-derivative Ω_D penalty for various choices of the smoothing parameters λ. For the smallest λ ($\lambda = 10^{-8}$), almost no penalty had any effect, and the classification is equivalent to that of LDA. The overall classification accuracy (number correctly classified divided by the number of test samples) is about 0.542 for LDA, but for PDA, the highest overall accuracy equals 0.750, 38.38% higher than that provided by the LDA method. We concluded that the penalty effectiveness for PDA is significant. As the level of smoothing increases, the accuracies of PDA improve until peaking and then decline. The optimal smoothing parameter λ value leading to the highest accuracy for PDA appears after corresponding training accuracy begins decreasing. This observation is consistent with that in Yu *et al.* (1999). Although classification accuracies for testing a range of λ values using the other two datasets are not shown for PDA, as in figure 3 here, we have observed similar behaviour performed by PDA.

Table 2 lists all overall classification accuracies (rates) produced using PDA from the three datasets, each with 10 spectral ranges. Each rate in the table, either for healthy, infected levels or for both averaged, is averaged from accuracies of three non-overlapping test sets. We used the hold-out sampling method to select test samples. We first randomly divided all samples in a dataset into three parts equally. We then used the 1st two parts as training samples and the 3rd part as a test sample (i.e. test set 1), and used the 1st and 3rd parts as training samples and the 2nd as test samples (i.e. test set 2) and the same rule was applied to test set 3. The average accuracy calculated from all 10 spectral ranges for each dataset is the highest for

APR02 (0.667), followed by JUL02 (0.633) and the lowest for SEP01 (0.610). Differences in spectral reflectance of plant material between samples are mainly caused by changes in biochemicals contained in plant leaves (Curran 1989, Elvidge 1990), especially pigment contents in the visible region and water content in the NIR and SWIR regions. Classification by PDA here is primarily based on the ratio of between-class spectral variance to within-class spectral variance. Therefore, by this point, the accuracy results for the three datasets seems reasonable when considering the relative water content (RWC) difference between the two health levels (table 3). The order of RWC difference between the two health levels for the three datasets parallels their accuracy order, i.e. RWC difference APR02 > JUL02 > SEP01 corresponding to raining season (late spring), dry season (summer) and very dry season (early fall). However, since the RWC differences of all three datasets are very small, the spectral difference of average spectra between the two health levels also is very slight (see figure 1). This has led to a lower overall average accuracy and a smaller accuracy difference among the three datasets analysed by PDA. When focusing on the accuracy differences calculated from the 10 spectral ranges, some higher accuracies are produced by those spectral range wavelengths shorter than 1400 nm (see italic numbers in table 2), especially those covering the visible and NIR regions only (APR02 and JUL02 datasets). We concur with Gong *et al.* (1997) and Van Aardt and Wynne (2001), who demonstrated that spectral information derived from shorter wavelengths favours classification. This spectral range is useful moreover because it is always available for laboratory spectra measurements. In addition, the use of all 2001 bands, covering 400–2400 nm, in this analysis does not guarantee the creation of the highest identification accuracy between the two health levels. In fact, for the PDA classification results, only the APR02 dataset produced the highest accuracy (0.750), and the other two datasets did not. When checking the classification accuracies generated with CCSM (table 4), we can easily note that the use of all 2001 bands does not produce the highest accuracies for all three datasets. This may be because some bands in classification have made a negative contribution to the final identification of the two health levels.

4.2 *CCSM*

With the same sampling split strategy to partition the three datasets into training sets and test sets as used for PDA, table 4 lists all classification accuracy results for CCSM from the three datasets for all 10 spectral ranges. In general, the overall average accuracies are lower than those produced by PDA (overall average 0.667 for PDA vs 0.561 for CCSM, 0.633 vs 0.585 and 0.610 vs 0.573). Moreover, the accuracy order also differs from that by PDA. The CCSM method produced the highest

Table 3. Relative water content (RWC) of three datasets of coast live oak leaves.

	Healthy RWC (%)		Infected RWC (%)		All RWC (%)	
Dataset	Average	SD	Average	SD	Average	SD
APR02	65.09	6.88	67.94	6.74	66.58	6.92
JUL02	45.72	2.90	46.06	2.51	45.90	2.70
SEP01	42.20	4.78	42.46	4.60	42.33	4.67

Table 4. Discriminant accuracies of three datasets at the two health levels using CCSM classifier.

No.	Wavelength range(nm)	APR02, N = 96			JUL02, N = 126			SEP01, N = 108		
		H-rate	I-rate	H-I ave	H-rate	I-rate	H-I ave	H-rate	I-rate	H-I ave
1	400–702	*0.58*	*0.69*	*0.633*	0.58	*0.68*	*0.633*	*0.56*	0.43	0.491
2	400–1002	*0.53*	0.58	0.558	*0.67*	0.58	*0.621*	*0.59*	0.54	0.565
3	707–1002	*0.53*	0.54	0.538	*0.70*	0.44	0.570	0.54	0.54	0.537
4	782–1372	0.51	0.46	0.485	*0.67*	0.58	*0.621*	0.50	0.59	0.546
5	502–1372	0.51	0.67	*0.589*	0.58	0.52	0.549	0.52	0.54	0.528
6	1007–2400	0.49	0.65	0.567	0.58	0.55	0.564	0.41	*0.81*	0.611
7	852–1897	0.51	0.58	0.547	0.57	0.55	0.556	0.41	*0.81*	*0.611*
8	1377–2400	0.49	0.63	0.557	0.52	*0.67*	0.592	0.41	*0.81*	*0.611*
9	1377–1897	0.49	0.60	0.547	0.55	0.65	0.601	0.41	*0.81*	*0.611*
10	400–2400	0.49	*0.69*	0.588	0.55	0.53	0.540	0.44	*0.80*	*0.620*
	Average	0.513	0.608	0.561	0.597	0.573	0.585	0.478	0.669	0.573

Note: H-rate and I-rate denote discriminant accuracies from healthy and infected samples, respectively; H-I ave is average of H-rate and I-rate. The italic numbers in the table indicate the first and second highest accuracy in each column.

discriminant accuracy from the JUL02 dataset while the accuracy generated from APR02 is the lowest. By comparing accuracy variation among all 10 spectral ranges, it is evident that some shortwave spectral ranges (wavelength shorter than 1400 nm) have also led to higher classification accuracies for all three datasets except for SEP01 discriminant accuracies for infected level. Again, this demonstrates that shortwave spectral information favours classification. There are spectral ranges that produced similar or identical classification accuracies (e.g. most spectral ranges in the SWIR region). We can explain this phenomenon by showing that similar spectral curve shapes among spectral samples that belong to one class, either healthy or infected. Figure 4 illustrates the similarity of the spectral curve shapes (plot data derived from SEP01 dataset). For the SWIR region in the figure, the shapes of all spectral curves look very similar, producing similar accuracies across spectral ranges numbers 5–9.

4.3 *Comparison of performance between PAD and CCSM*

In the spectroscopic determination of the two health levels of coast live oak, healthy and infected, with laboratory-measured spectra, PDA performs significantly better than CCSM. However, both classification accuracies are not ideal (an acceptable classification accuracy generally being around 80%). PDA can highlight spectral difference information stored in narrow bands, especially for those bands with wavelengths shorter than 1400 nm; the method effectively uses the subtle spectral difference information to identify a spectral sample as either at healthy level or infected level. The orders of the accuracies derived by the PDA method for all seasons are consistent with the order of the RWC difference between the two health levels for all three datasets. In other words, the spectral variation caused by different RWCs can be efficiently discerned by the PDA method. Fundamentally, CCSM effectively uses the similarity of two curve shapes to classify samples instead of using spectral differentiation. Therefore its classification accuracy is not related to the spectral difference caused by RWC variation or other biochemical changes in our datasets. In this study, laboratory-measured spectra, whose curves all look very

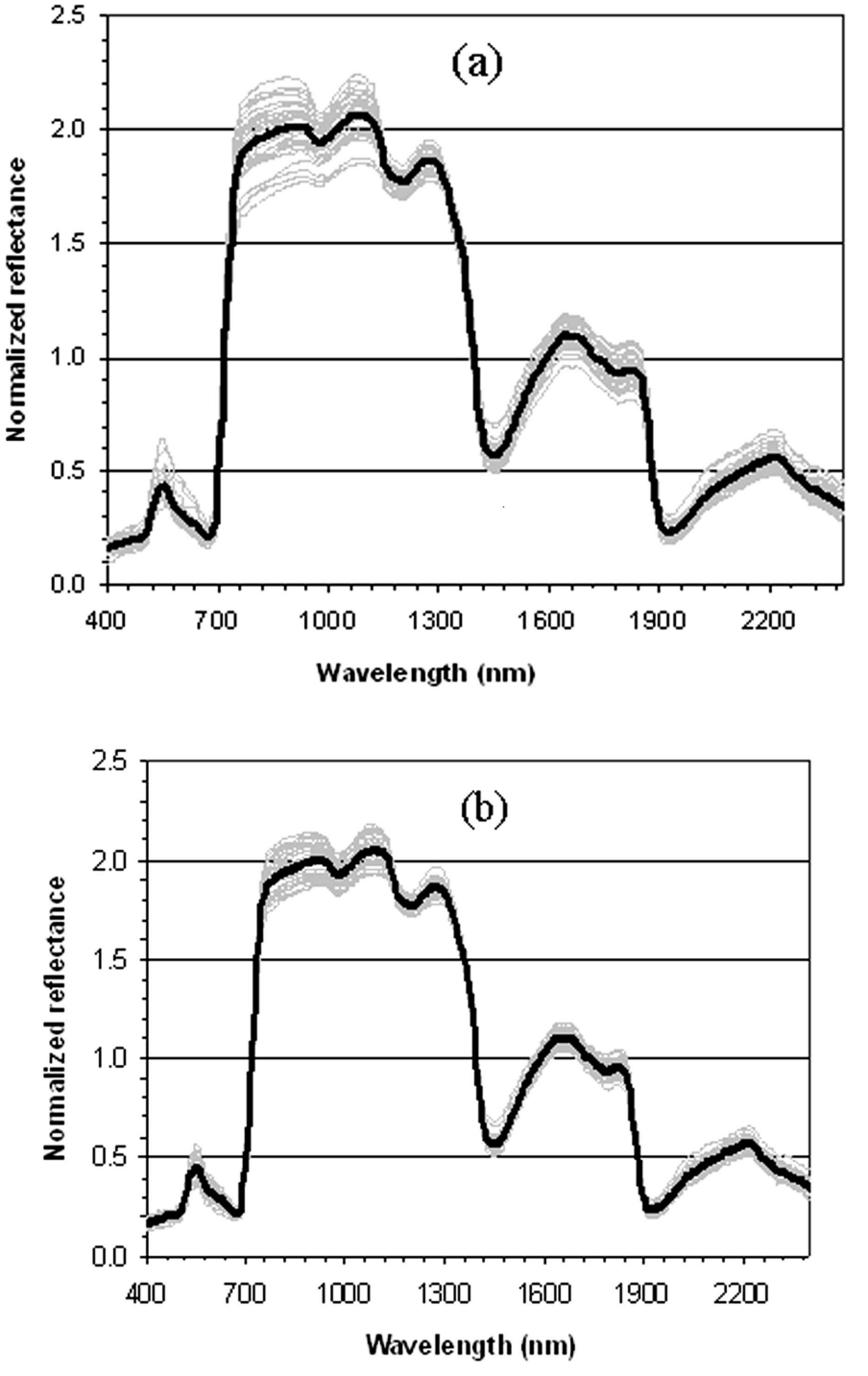

Figure 4. Mean spectra of the two health levels: healthy (*a*) and infected (*b*), calculated from the SEP01 dataset, in association with individual spectral samples showing the individual spectral variation around their mean spectra.

similar, may not be suitable for CCSM to determine a spectral sample labelling (i.e. either healthy or infected). In comparison with the result by LDA ($\lambda \approx 0$ in figure 3), PDA has proven that it should be a promising discriminant analysis method.

5. Discussion

In general, the reflectance spectra of green and yellow leaves in those absorption bands centred at 970 nm, 1200 nm, 1450 nm and 1940 nm are quickly saturated and solely dominated (Elvidge 1990) by changes in leaf water content. However, for the coast live oak leaves, based on our preliminary analysis (Pu *et al.* 2003, 2004), the reflectances at bands 970 nm and 1200 nm are related to leaf RWC and not saturated even if the leaf RWC is high—up to 60%. In other words, a spectral range including the two minor water absorption bands (970 nm and 1200 nm) might be more useful for separating the two health levels spectrally than that including the two major water absorption bands (1450 nm and 1940 nm). In fact, figure 1 clearly shows that the spectral range with wavelength shorter than 1400 nm has a greater spectral difference (note the spectral range from 700 nm to 1300 nm) between the two health levels than that with wavelength longer than 1400 nm (note the spectral range from 1400 nm to 2000 nm). Therefore, it should be reasonable (see table 2) that some shortwave spectral ranges (wavelength shorter than 1400 nm) have led to higher classification accuracies for all three datasets except for SEP01 discriminant accuracies at infected level.

It is evident that reflectance spectra of oak leaves are related to leaf RWC (figure 1), at least in the NIR and middle IR ranges. In the NIR range, the high leaf RWC can cause higher spectral reflectance. This is because the full cell of oak leaves, caused by the pulling force of water in the cell, is favourable for increasing the reflected spectrum in the range. However, in the middle IR (including the two major water absorption bands), due to the strong water absorption function, the spectral reflectance decreases when the leaf RWC increases. The APR02 and JUL02 datasets in figure 1 have clearly proven this point. The spectral reflectance curves of both datasets have shown that the reflectance of the infected samples due to higher leaf RWC (table 3) is higher in the NIR range and lower in the middle IR range than those of health samples due to lower leaf RWC. For the SEP01 dataset, it seems that the opposite result appears. We do not exactly know why, but it may be related to almost the same leaf RWC for the two health levels and to spectral measurement error (e.g. not perfect spectral calibration).

Remote sensing of SOD diseased trees for identifying various health levels is based on spectral differences between them. It is possible that this difference is caused by changes in pigment content, water content, other biochemical constituents and cell structure in the oak leaves. Little is known about the biochemical change occurring in the oak leaves of infected trees. Most studies examining SOD canker disease describe symptoms appearing on trunks early, while the canopy change occurs much later in the disease cycle (McPherson *et al.* 2000, Rizzo *et al.* 2002). We compared the RWC of healthy and infected coast live oak leaves (table 3).

The RWC difference between healthy and infected samples for the three datasets is not significant when considering corresponding standard deviations to their means. This means that it will be difficult to rely on spectral changes caused by RWC to diagnose the health levels in trees (referring to the classification results in tables 2 and 4). SOD infected oak leaves at the late stage of the disease show colour change in the

leaves or a chlorotic appearance that may primarily be attributed to leaf moisture stress. If this is true, infected leaves gathered from late state infected trees should have a lower RWC than that of healthy leaves. However, based on our measurements (table 3), at an early stage of the infection, infected leaves conversely have a slightly higher RWC than healthy leaves. This phenomenon supports the work by Skiecki and Bernhardt (2002). They found that trees with early SOD symptoms tended to have higher stem water potentials (SWPs) (and therefore higher RWCs in leaves) than trees without SOD symptoms. Furthermore, as long as the trees remain green, SWP does not seem to decrease gradually over time as symptoms progress on the stem. While Skiecki and Bernhardt (2002) assume that some time in the year preceding canopy colour change the moisture content of the leaves declines, they cannot be sure of the time. It is entirely possible that the RWC of infected leaves remains unchanged over a relatively long time period, then rapidly changes immediately prior to and precipitating the dramatic colour change. Therefore, at the early stages of SOD, the results showing the RWC of infected leaves as higher than or equivalent to that of healthy leaves seems reasonable.

There have been many studies on forest moisture stress detection and mapping with multi/hyperspectral remote sensing data, including both airborne and satellite remote sensing. Water stress may be attributed to drought (either weather or soil) or diseases or both. A general conclusion drawn from this type of research suggests that canopy moisture stress would be detectable with remote sensing techniques only when the moisture stress reaches a relatively high level. For example, Riggs and Running (1990) used Airborne Imaging Spectrometer (AIS-2) data to detect canopy water stress in conifers, and they concluded that water stress in conifer canopies may not be routinely detectable at an operational landscape scale because no significant differences in reflectance between most coniferous stressed and controlled canopies were found, probably due to the relatively weak water stress. For mapping mixed conifer mortality due to continuous drought in the Lake Taheo Basin with multi-temporal Landsat TM images, Collins and Woodcock (1994, 1996) employed several change detection techniques to successfully detect mortality trees. These trees died because of severe drought (high moisture stress), thus they are very detectable. In monitoring forest health conditions, especially for hardwood oak forest diseases, airborne digital imageries have been successfully used to delineate or map dead and dying oak trees (Kelly 2002) in monitoring SOD in California and to detect oak wilt disease (Everitt *et al.* 1999) in south-central Texas. In addition, satellite images are also feasible to detect defoliation in hardwood forests with SPOT imagery (e.g. Muchoney and Haack 1994) and in conifer forests with Landsat TM data (e.g. Royle and Lathrop 1997). However, the defoliation has to be $>25\%$. This defoliation can be caused by canopy water stress, insects and diseases. All previous work has demonstrated that by using airborne or satellite remote sensing images, canopy moisture stress may be detected only when the stress is very high, and forest healthy conditions can be monitored or mapped only for those severely infected (or affected) trees and dying or dead trees. To detect or monitor slight moisture stress on canopy or some forest diseases at an early stage when the canopies still look green, existing remote sensing techniques may not be adequate.

Our experiment results, using laboratory-measured spectra to differentiate the two health levels of coast live oak leaves, also prove to a certain degree that the RWC of infected leaves is not very different from that of healthy leaves (i.e. all green leaves), therefore remote sensing diagnosis of SOD at early stages at individual tree level or

stand level may not be feasible. However, because the stressed or infected trees can eventually change the tree leaf colour and canopy structure, expressed as changes in leaf area index, crown closure and stem density, etc., and because this change should affect spectral characteristics at canopy and landscape scales (Tucker 1979, Everitt *et al*. 1986), it might be expected that remote sensing of plant canopy stress should be feasible at an advanced stage. Especially as remote sensing technology improves in spectral, spatial and temporal resolutions and in the ratio of signal to noise of images, it will become a very promising tool to monitor and map forest moisture stress and other healthy conditions at various levels.

6. Preliminary conclusions

In this study, we assumed the slight spectral difference between the two health levels, healthy and infected, might be caused mainly by differences in the relative water contents (RWCs) of oak leaves at the two health levels, even though the difference is very small. In the NIR range, the high leaf RWC can cause higher spectral reflectance due to multi-reflected effectiveness of cell structure. However, in the middle IR (including the two major water absorption bands), the spectral reflectance decreases when the leaf RWC increases due to the strong water absorption function.

In this experiment, penalized discriminant analysis (PDA) has shown its advantage over cross correlogram spectral matching (CCSM) for discriminating samples of coast live oak leaves across three seasons. The overall average accuracy for PDA is approximately 7% higher than that for CCSM. PDA catches spectral difference information primarily caused by RWC differences in healthy and infected leaves, while CCSM can effectively use the similarity of spectral curve shapes between a test spectrum and a reference spectrum. The accuracies produced by both algorithms are very low, and could even be considered unacceptable from a routinely operational point of view. However, when we consider the spectral similarity among spectral samples, we conclude that PDA should be a very promising classification algorithm compared to traditional linear discriminant analysis (LDA), which is often problematic for classification with hyperspectral data. Among the 10 spectral ranges, some higher accuracies are produced by both PDA and CCSM algorithms from those spectral range wavelengths shorter than 1400 nm, especially from those covering visible and NIR regions only (APR02 and JUL02 datasets).

Based on our experimental results and previous work, existing remote sensing techniques, including airborne or satellite remote sensing and multispectral or hyperspectral remote sensing, may be insufficient for monitoring and mapping disease-induced moisture stress in trees that have recently been infected. However, this does not preclude the analysis of trees at very advanced stages of disease, and the practicality of finding trees within weeks of dying is considerable.

Acknowledgements

This research was partially funded by a NASA EO-1 Science Validation Grant NCC5-492, and the NASA New Investigator Program. Additional support came from the California Department of Forestry and Fire Protection. We would like to thank Brice McPherson, Shaokui Ge, Dave Graham-Squire, Yong Tian, Qian Yu

and Desheng Liu for their help in field sampling and spectral and weight measurements in the laboratory. This work was performed at the Center for the Assessment and Monitoring of Forest and Environmental Resources, Berkeley, CA, USA.

References

COLLINS, J.B. and WOODCOCK, C.E., 1994, Change detection using the Gramm-Schmidt transformation applied to mapping forest mortality. *Remote Sensing of Environment*, **50**, 267–279.

COLLINS, J.B. and WOODCOCK, C.E., 1996, An assessment of several linear change detection techniques for mapping forest mortality using multitemporal Landsat TM data. *Remote Sensing of Environment*, **56**, 66–77.

CURRAN, P.J., 1989, Remote sensing of foliar chemistry. *Remote Sensing of Environment*, **30**, 271–278.

ELVIDGE, C.D., 1990, Visible and near infrared reflectance characteristics of dry plant materials. *International Journal of Remote Sensing*, **11**, 1775–1795.

EVERITT, J.H., RICHARDSON, A.J. and NIXON, P.R., 1986, Canopy reflectance characteristics of succulent and nonsucculent rangeland plant species. *Photogrammetric Engineering and Remote Sensing*, **52**, 1891–1897.

EVERITT, J.H., ESCOBAR, D.E., APPEL, D.N., RIGGS, W.G. and DAVIS, M.R., 1999, Using airborne digital imagery for detecting oak wilt disease. *Plant Disease*, **83**, 502–505.

GARBELOTTO, M., SVIHRA, P. and RIZZO, D.M., 2001, Sudden Oak Death syndrome fells three oak species. *California Agriculture*, **55**, 9–19.

GONG, P., PU, R. and YU, B., 1997, Conifer species recognition: an exploratory analysis of *in situ* hyperspectral data. *Remote Sensing of Environment*, **62**, 189–200.

GONG, P., PU, R. and YU, B., 2001, Conifer species recognition: effects of data transformation. *International Journal of Remote Sensing*, **22**, 3471–3481.

HASTIE, T., BUJA, A. and TIBSHIRANI, R., 1995, Penalized discriminant analysis. *Annual Statistics*, **23**, 73–102.

KELLY, N.M., 2002, Monitoring Sudden Oak Death in California using high-resolution imagery. *Proceedings of the Fifth Symposium on Oak Woodlands: Oak in California's changing landscape*, 23–25 October 2001, San Diego, California, USDA-Forest Service, General Technical Report PSW-GTR-184, pp. 799–810 (Berkeley, CA: Pacific Southwest Forest and Range Experimental Station).

KELLY, M. and MEENTEMEYER, R., 2002, Landscape dynamics of the spread of Sudden Oak Death. *Photogrammetric Engineering and Remote Sensing*, **68**, 1001–1009.

MCPHERSON, B.A., WOOD, D.L., STORER, A.J., SVIHRA, P., RIZZO, D.M., KELLY, N.M. and STANDIFORD, R.B., 2000, Oak mortality syndrome: sudden death of oaks and tanoaks. *Tree Notes*, **26**, 1–6.

MUCHONEY, D.M. and HAACK, B.N., 1994, Change detection for monitoring forest defoliation. *Photogrammetric Engineering and Remote Sensing*, **60**, 1243–1251.

PU, R., GE, S., KELLY, N.M. and GONG, P., 2003, Spectral absorption features as indicators of water status in coast live oak (*Quercus Agrifolia)* leaves. *International Journal of Remote Sensing*, **24**, 1799–1810.

PU, R., FOSCHI, L. and GONG, P., 2004, Spectral features analysis for assessment of water status and health level in Coast Live Oak (*Quercus Agrifolia)* leaves. *International Journal of Remote Sensing*, **25**, 4267–4286.

RIGGS, G.A. and RUNNING, S.W., 1990, Detection of canopy water stress in conifers using the Airborne Imaging Spectrometer. *Remote Sensing of Environment*, **35**, 51–68.

RIZZO, D.M., GARBELOTTO, M., DAVIDSON, J.M., SLAUGHTER, G.W. and KOIKE, S.T., 2002, *Phytophthora ramorum* as the cause of extensive mortality of *Quercus* spp. and *Lithocarpus densiflorus* in California. *Plant Disease*, **86**, 205–214.

ROYLE, D.D. and LATHROP, R.G., 1997, Monitoring hemlock forest health in New Jersey using Landsat TM data and change detection techniques. *Forest Science*, **43**, 327–335.

SKIECKI, T. and BERNHARDT, E., 2002, Evaluation of stem water potential and other tree and stand variable as risk factors for *Phytophthora ramorum* canker development in coast live oak. *Proceedings of the Fifth Symposium on Oak Woodlands: Oak in California's changing landscape*, 23–25 October 2001, San Diego, California, USDA-Forest Service, General Technical Report PSW-GTR-184, pp. 787–798 (Berkeley, CA: Pacific Southwest Forest and Range Experimental Station).

TUCKER, C.J., 1979, Red and photographic infrared linear combinations for monitoring vegetation. *Remote Sensing of Environment*, **8**, 127–150.

VAN AARDT, J.A.N. and WYNNE, R.H., 2001, Spectral separability among six southern tree species. *Photogrammetric Engineering and Remote Sensing*, **67**, 1367–1375.

VAN DER MEER, F. and BAKKER, W., 1997, Cross correlogram spectral matching: application to surface mineralogical mapping by using AVIRIS data from Cuprite, Nevada. *Remote Sensing of Environment*, **61**, 371–382.

VAN DER MEER, F. and BAKKER, W., 1998, Validated surface mineralogy from high-spectral resolution remote sensing: a review and a novel approach applied to gold exploration using AVIRIS data. *Terra Nova*, **10**, 112–119.

YU, B., OSLAND, I.M., GONG, P., and PU, R., 1999, Penalized discriminant analysis of *in situ* hyperspectral data for conifer species recognition. *IEEE Transactions on Geoscience and Remote Sensing*, **37**, 2569–2577.